물분해 시스템 효율/안정성 유지 이슈
Efficiency and Stability Issues in Water Splitting System

Uk Sim, Ph. D.

Nanomaterials for Energy & Environment Laboratory
www.uksim.org

A polydopamine-mediated biomimetic facile synthesis of molybdenum carbide-phosphide nanodots encapsulated in carbon shell for electrochemical hydrogen evolution reaction with long-term durability

Published

Tae-Yong An [a], Subramani Surendran [a], Hyunkyu Kim [a], Woo-Seok Choe [b], Jung Kyu Kim [b,**], Uk Sim [a,*]

Molybdenum based catalysts

Adv. Funct. Mater. 2017, 27, 1703933

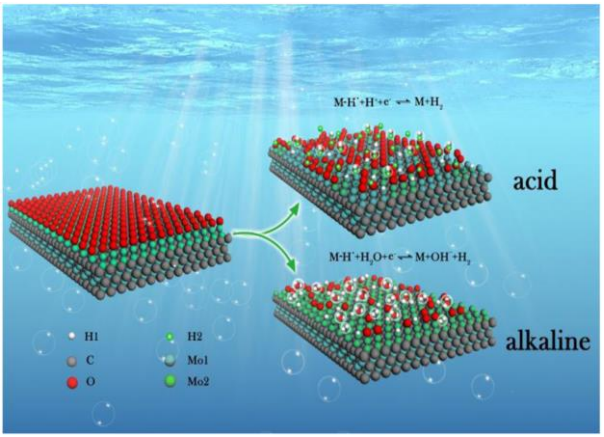

ACS Appl. Mater. Interfaces 2018, 10, 40500−40508

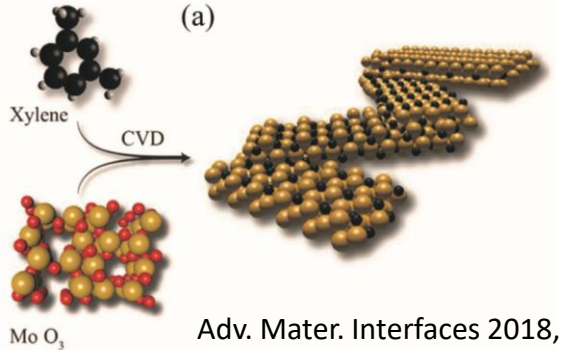

Adv. Mater. Interfaces 2018, 1701113

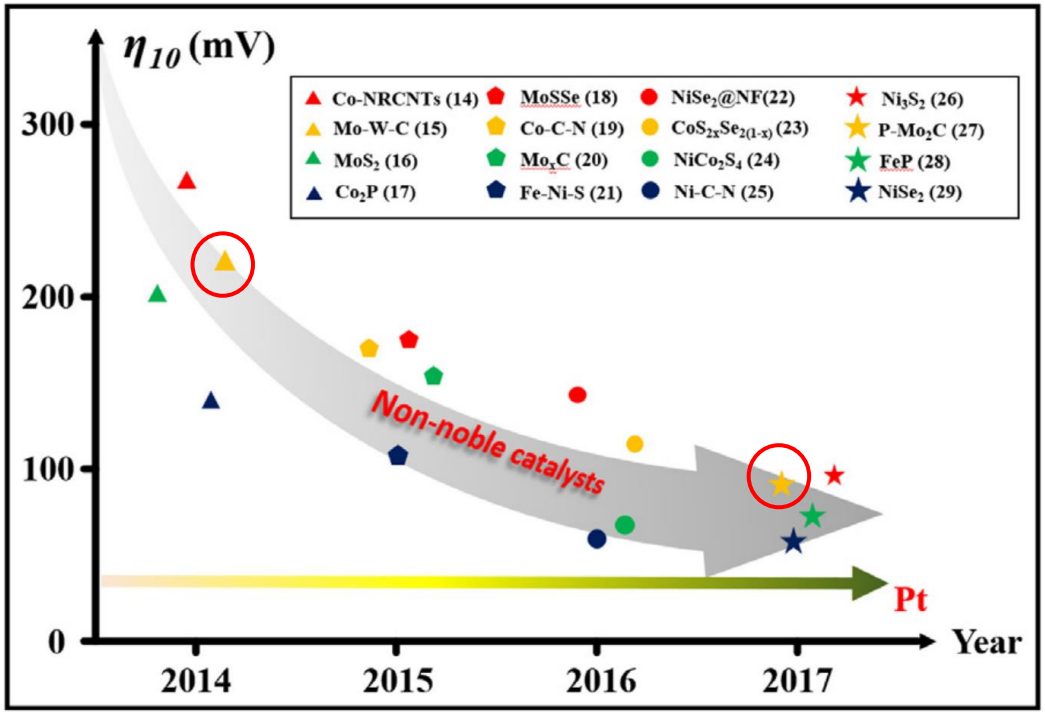

Curr Opin Electrochem,2018,7:7-14

- **Molybdenum-based catalysts** have the characteristics of non-precious, environmentally benign, and corrosion resistant catalysts.
- **Mo_2C** is stable and has excellent activity under basic conditions.

Polydopamine

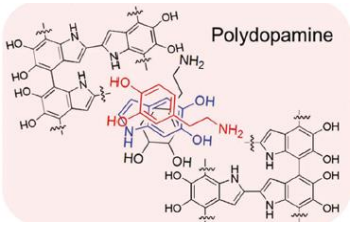

- Eco-friendly chelating agent.
- A facile polymerization process.
- Excellent conductivity after carbonization through annealing.
- Providing rich nitrogen and carbon sources.

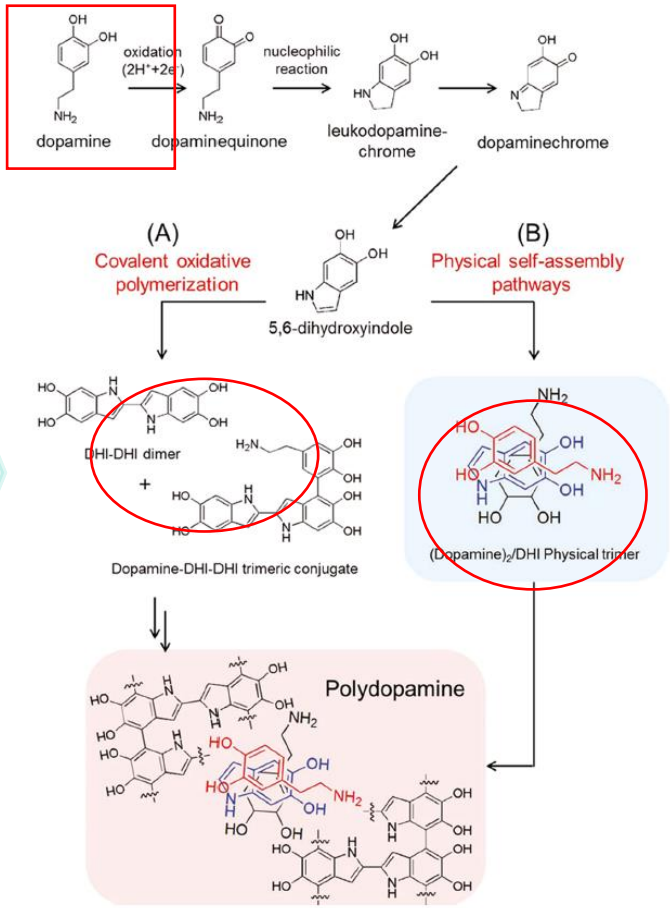

Adv. Funct. Mater. 2012, 22, 4711.

Mo_2C-MoP nanodots encapsulated in carbon shell for HER

Composites Part B 175 (2019) 107071

➢ X-ray diffraction patterns

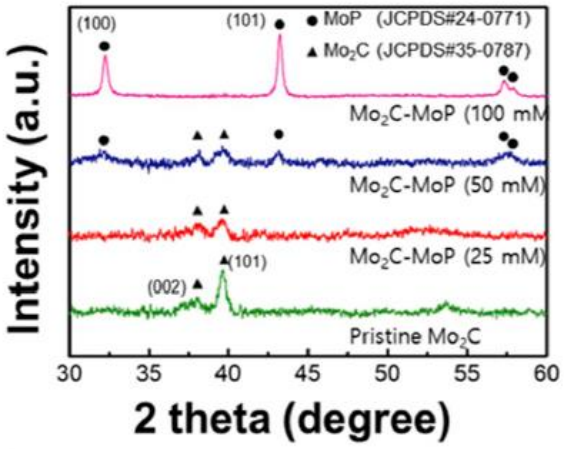

- The diffraction peaks of the Mo_2C–MoP@CP (25 mM) sample revealed that no MoP peaks were observed in the XRD pattern of the sample owing to its P deficiency.
- Mixed Mo_2C and MoP phases were observed in the spectrum of Mo_2C–MoP@CP (50 mM), and the obtained diffraction peaks were consistent with orthorhombic Mo_2C and hexagonal MoP, respectively.
- The standard peaks of Mo_2C diminished in the spectrum of Mo_2C–MoP@CP (100 mM), which substantiated the formation of highly crystalline hexagonal MoP nanoparticles.

➢ X-ray photoelectron spectroscopy spectra

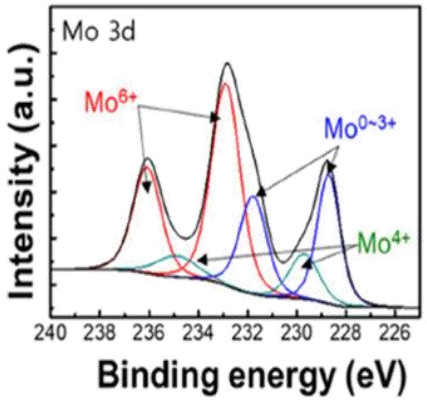

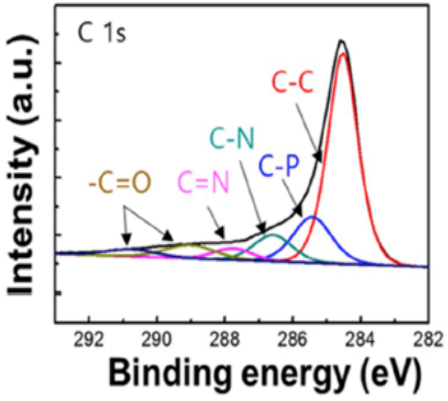

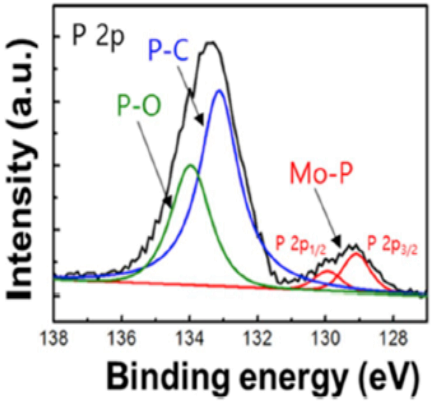

- The significant C–N and C=N peaks imply that the carbon shell from the carbonization of polydopamine was doped with nitrogen species.

Mo_2C-MoP nanodots encapsulated in carbon shell for HER

Composites Part B 175 (2019) 107071

➢ TEM images and EDS mappings

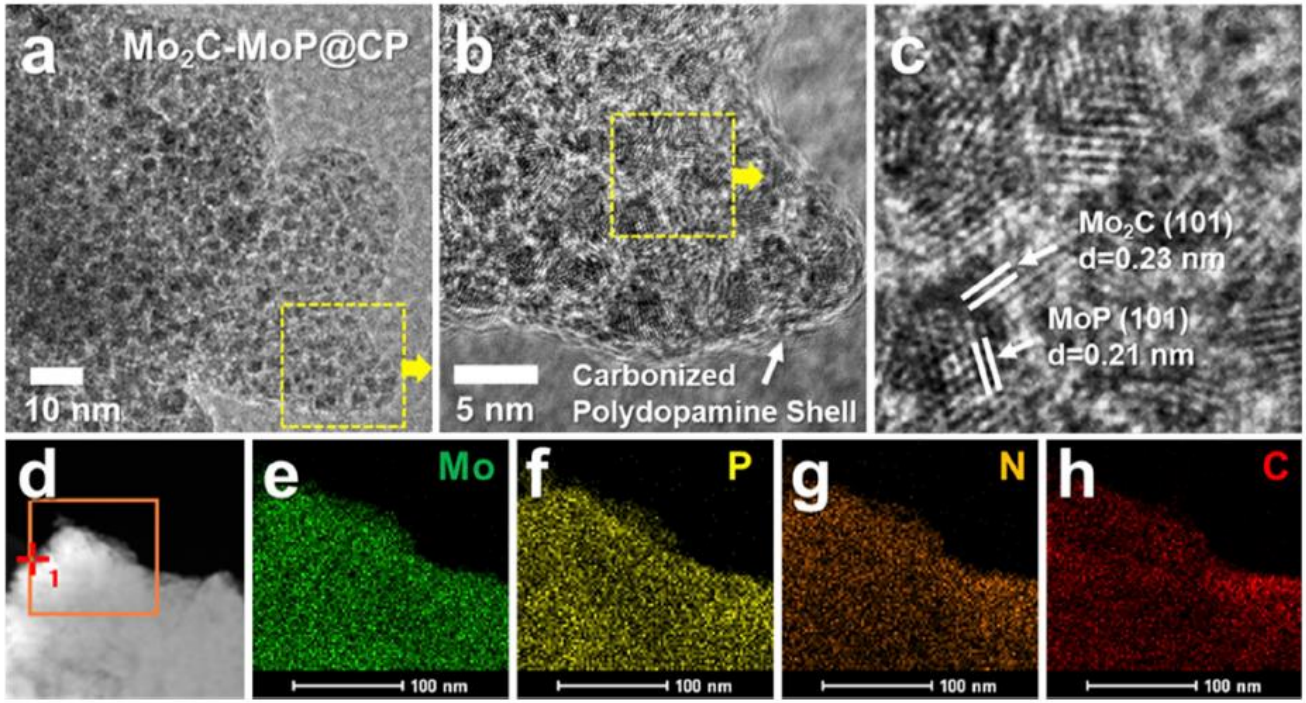

- The uniform distribution of N and C implied that the carbonized polydopamine shell consisted of N-doped C since polydopamine was an abundant source of N and C.
- The carbonization of polydopamine induced N doping on C, which could result in the high electronic conductivity and intra-connectivity of the Mo_2C–MoP@CP hybrid nanodots and thereby enhanced their reaction kinetics.

- Mo_2C–MoP@CP nanodots 3–5 nm in diameter were uniformly distributed on the surface and were separated from each other.
- Mo_2C–MoP@CP comprised a conformal coating of N-doped carbon shell that coated the Mo_2C–MoP hybrid nanodots.
- The resolved lattice spacings of 0.23 and 0.21 nm can be observed and are in good agreement with the d-spacings of the orthorhombic Mo_2C (101) and hexagonal MoP (101) phases, respectively.

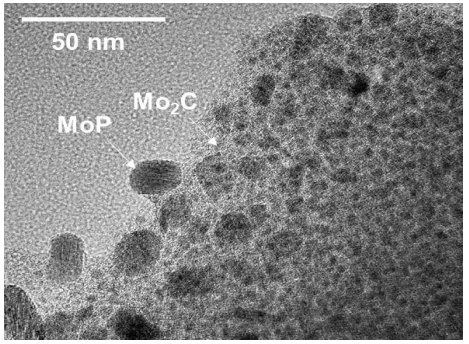

Mo_2C-MoP nanodots encapsulated in carbon shell for HER

Composites Part B 175 (2019) 107071

➢ Electrochemical data of HER performance

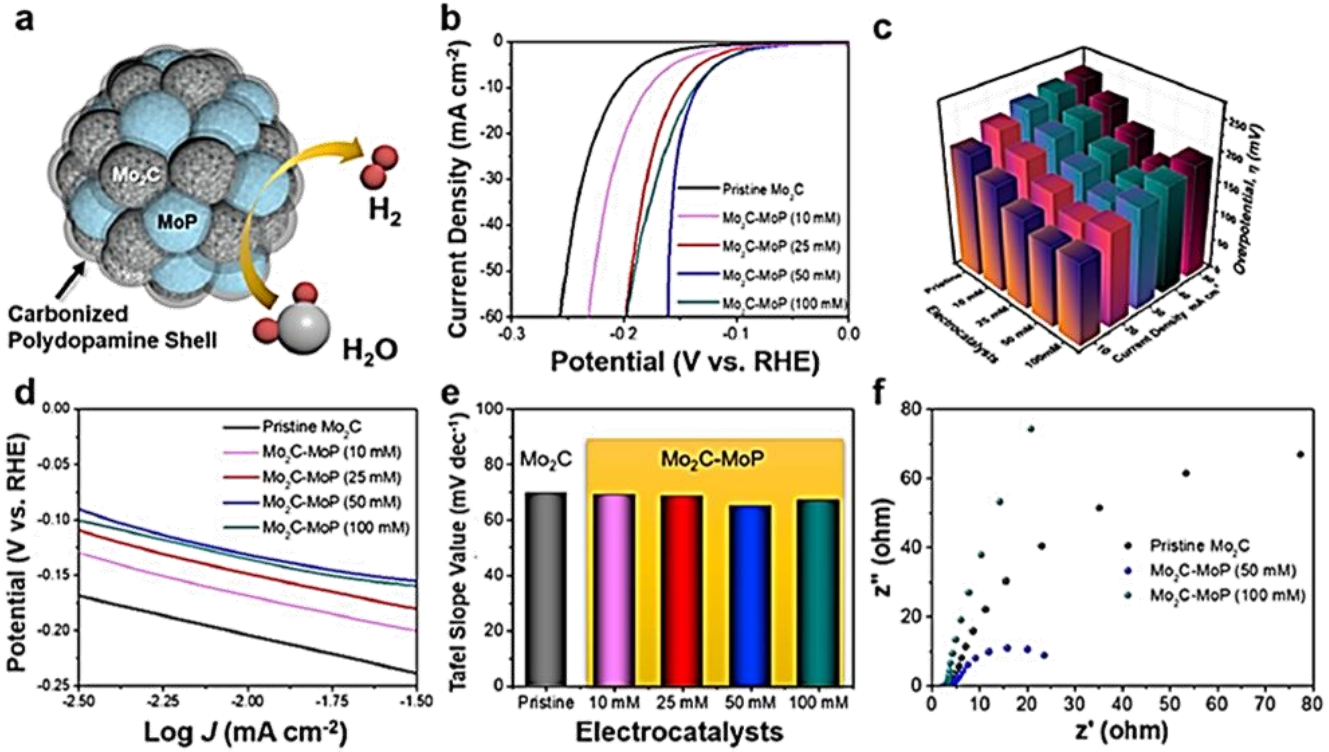

- As the concentration of ammonium dihydrogen phosphate (elemental P) was increased to 50 mM, the current density-potential (J-V) curve shifted approximately 77 mV toward the positive potential compared to that of pristine Mo_2C. The onset potential also positively shifted by 23 mV.

- A significant decrease in the Tafel slope (4.67 mV) from 69.59 mV dec^{-1} for the pristine Mo2C to 64.92 mV dec^{-1} for Mo_2C–MoP (50 mM) demonstrated the high electrochemical HER performance of Mo_2C–MoP@CP bound to 50 mM of P.
- In Nyquist plot, the semicircle of Mo_2C–MoP@CP (50 mM) was smaller than that of pristine Mo_2C, which indicated that the resistance of Mo_2C–MoP@CP (50 mM) was much lower than that of pristine Mo_2C, and therefore, provided favorable charge transport or transfer for efficient HER.

The synergistic effect of nitrogen and fluorine co-doping in graphene quantum dot catalysts for full water splitting and supercapacitor

Published

Yelyn Sim[a,1], Seung Jae Kim[b,1], Gnanaprakasam Janani[a], Yujin Chae[a], Subramani Surendran[a], Hyunkyu Kim[a], Seungryul Yoo[c], Dong Chan Seok[c], Yong Ho Jung[c], Cheolho Jeon[b], Joonhee Moon[b,*], Uk Sim[a,*]

Nitrogen and Fluorine co-doping in Graphene Quantum Dot for Water Splitting

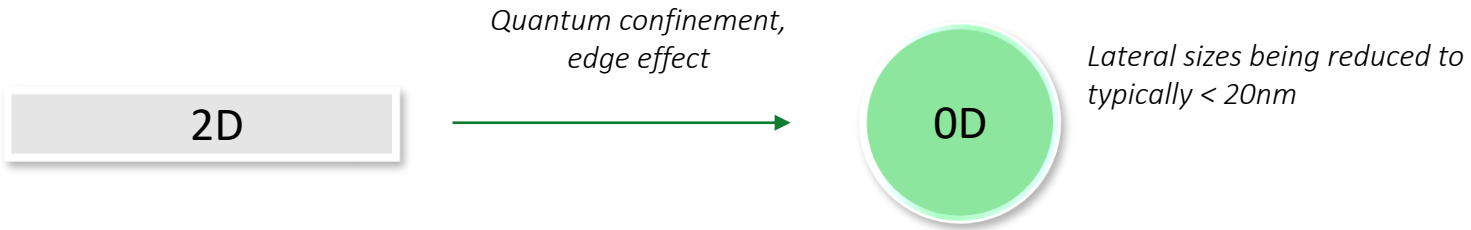

intralayer ------> *Strong covalent*

interlayer ------> *Weak van der Waals*

◆ Advantage of 0D materials **(quantum dots)**

- *Edge abundant features*
- *Larger surface-to-volume ratio*
- *Better solubility in both aqueous and nonaqueous solvent*
- *Higher tunability in both aqueous and nonaqueous solvents*
- *Higher tunability in physiochemical properties*
- *Better amenability to hybridize with other nanomaterials*
- *Ease to be doped and functionalized*

Nitrogen and Fluorine co-doping in Graphene Quantum Dot for Water Splitting

Nitrogen doping effects

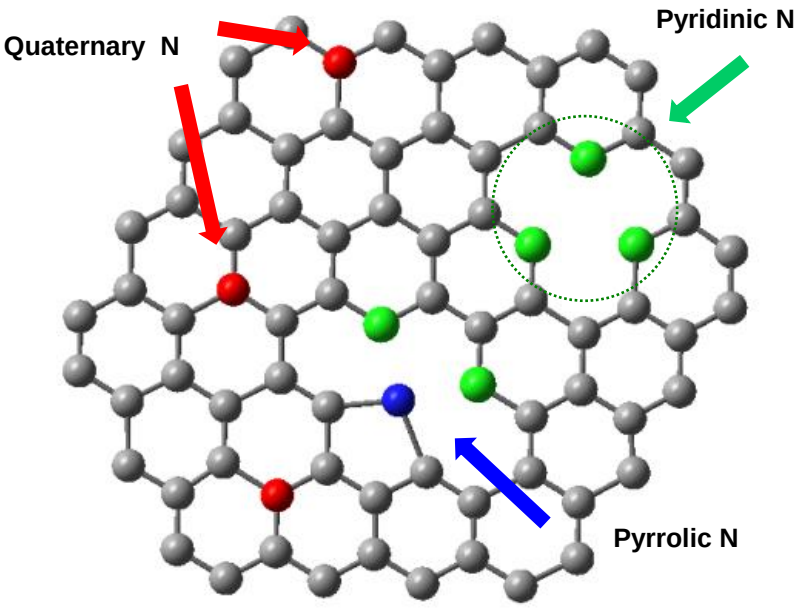

- *GQD with chemically bonded N atoms could alter their electronic characteristics and offer more active sites*
- *carbon adjacent to an N atom can cause a positive shift in Fermi energy, which was a benefit for the charge transfer*

- *Pyridinic : N atoms at the edge of six-membered ring*
- *Pyrrolic : N atoms at the edge of five-membered ring*
- *Graphitic : the substitutional site in graphene plane*
- *As the nitrogen doping time increases, the order of pyridinic, pyrrolic and others dominant.*
- *The doping to pyridinic and pyrrolic sites increases the work function*

Nitrogen and Fluorine co-doping in Graphene Quantum Dot for Water Splitting

Fluorine doping effects

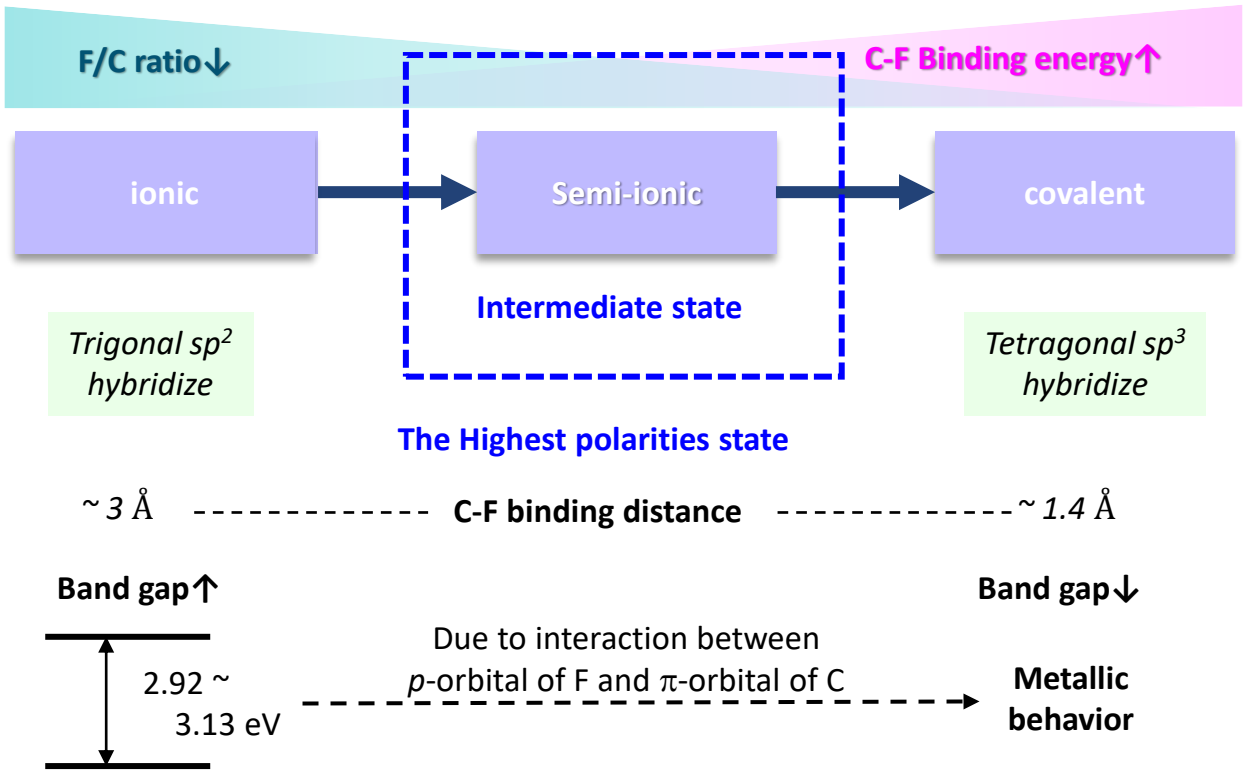

- *fluorine functionalization could alter the electronic state*
- *the bonding interaction between C and F can change ionic, semi-ionic, and covalent configurations owing to the strong electronegativity of fluorine*
- *With increasing F/C ratio, the C-F bonds change their character from ionic to semi-ionic to covalent one.*
- *the semi-ionic C-F bonding doped with ~4% fluorine could enhance the electrical properties of the electrode and facilitate electron transport through the active material*

N,F-GQDs for water splitting

Applied Surface Science 507 (2020) 145157

➢ AFM images of the GQDs dispersed of a SiO_2 substrate and height profiles

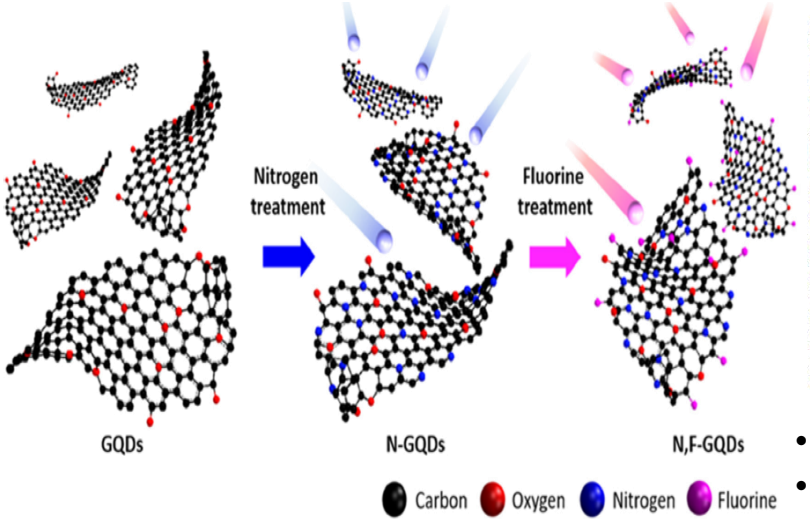

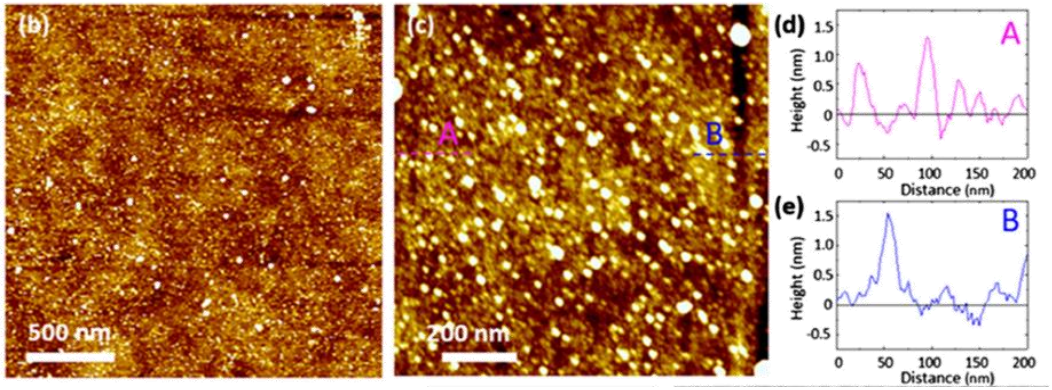

- Homogeneous N,F-GQDs particles were uniformly placed on the Si.
- An average under 1.5 nm height of N,F-GQDs, which indicates the number of layers in N,F-GQDs was about ~ 3 layers.

➢ TEM images and histogram showing the size distribution of GQDs

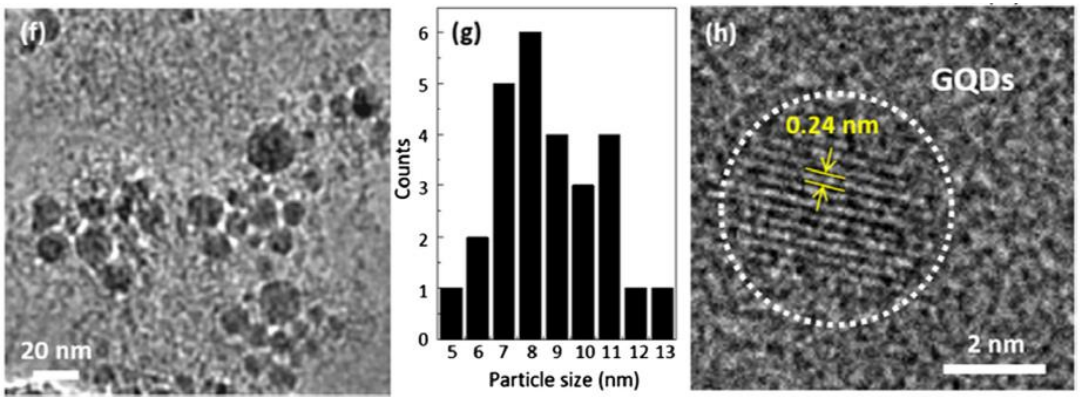

- Most of N,F-GQDs dispersed on graphene sheet show a size distribution from 2 to 10 nm with an average size of 8.7 nm.
- The lattice structure shown in the high-resolution TEM image indicates the N,F-GQDs are highly crystalline.

N,F-GQDs for water splitting

- FT-IR spectra and wide-scan XPS spectra

Applied Surface Science 507 (2020) 145157

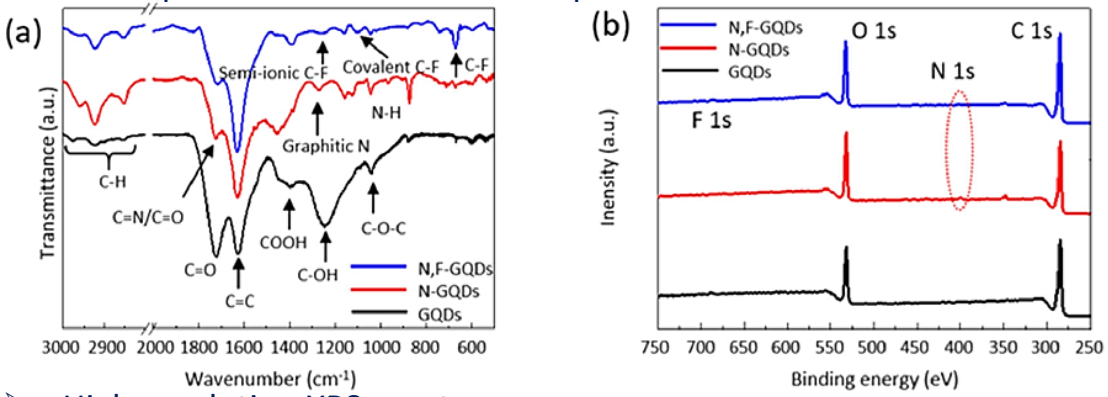

- High-resolution XPS spectra

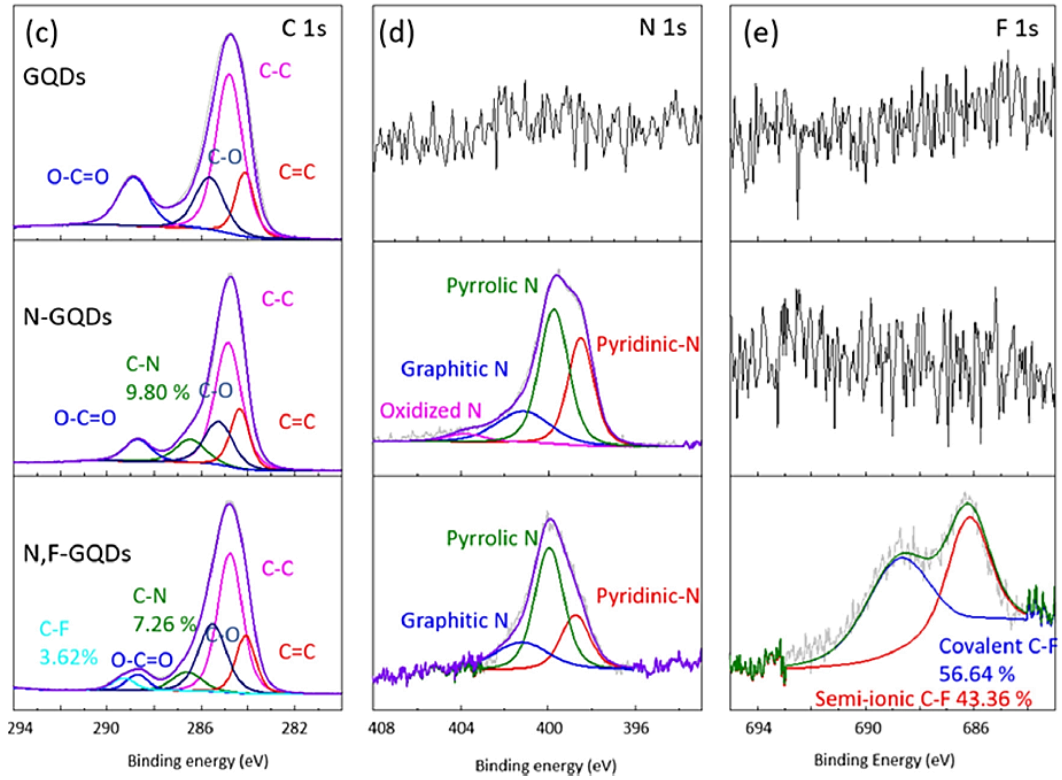

- N,F-GQDs shows three additional peaks at around 1250, 1100, and 670 cm^{-1} assigned to stretching vibration of semi-ionic C-F, covalent C-F, and C-F deformation vibration.
- Wide-scan XPS spectra reveal carbon, nitrogen, oxygen, and fluorine peaks at 282.4, 400.8, 532.8, and 686.8 eV, respectively.
- TheGQDs contains oxygen-rich functional groups without nitrogen and fluorine species.
- The N 1s peak exhibits three peaks at 398.5 (pyridinic N), 399.8 (pyrrolic N), and 401.1 eV (graphitic N), respectively, which nitrogen is successfully functionalized on N-GQD and N,F-GQDs.
- In the F 1s spectra, C-F bond consisting of covalent C-F bond (688. 8 eV) and semi-ionic C-F bond (686.2 eV) was only observed in the N,F-GQDs.

N,F-GQDs for water splitting

Applied Surface Science 507 (2020) 145157

➢ Electrocatalytic performance using 3-electrode system

LSV polarization curves for HER

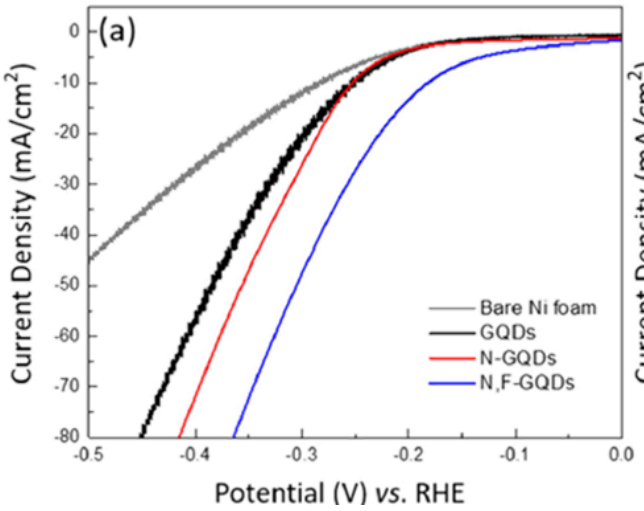

LSV polarization curves for OER

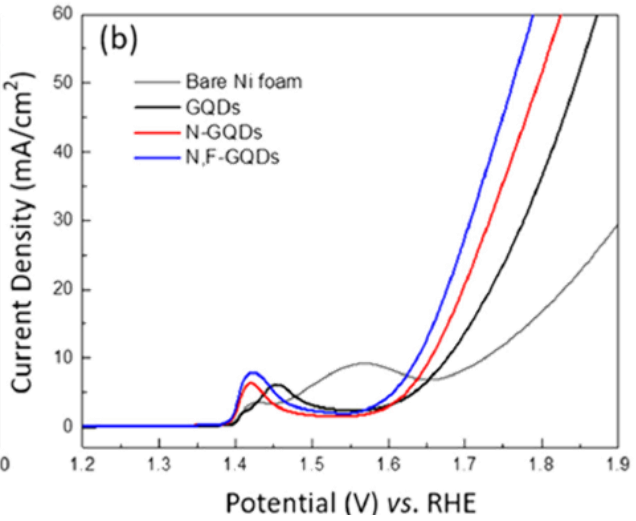

Stability test

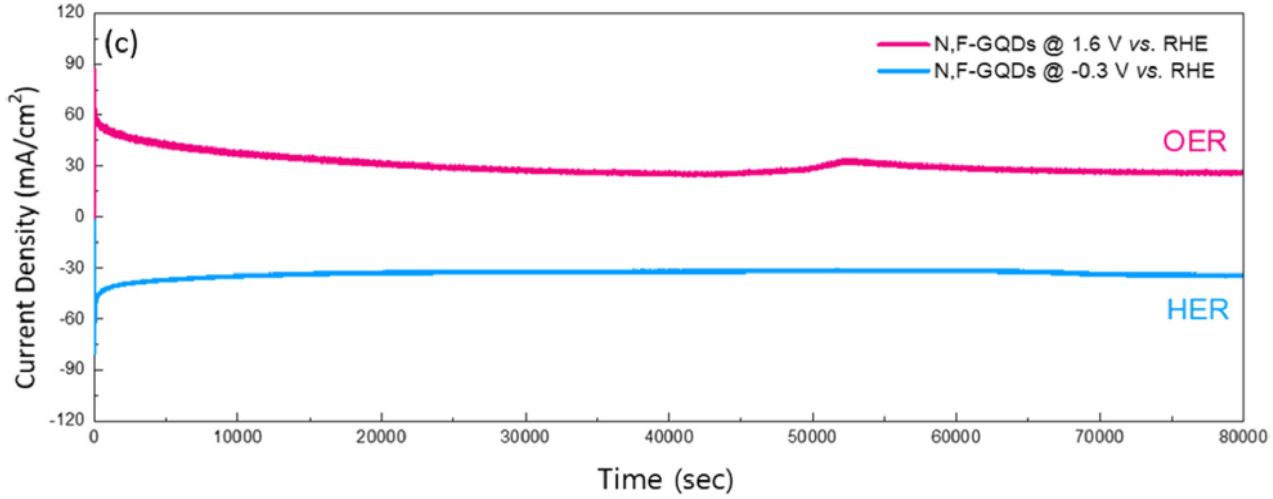

- In HER, the prepared N,F-GQDs electrocatalysts shows the lowest overpotential at 0.13 V where there indicates the current density of 10 mA cm^{-2}, while the N-GQDs, GQDs, and Ni foam require an equivalently high overpotential of 0.25 V, 0.26 V, and 0.29 V, respectively.
- In OER, the N,F-GQDs requisite a low overpotential of 0.4 V to generate a current density of 10 mA cm^{-2}, while the N-GQDs and GQDs electrocatalysts required higher overpotential to attain the similar current density.
- From the attained result of stability for both reaction, the N,F-GQDs is consistent without any loss of the current density for 80,000 s.

N,F-GQDs for water splitting

Applied Surface Science 507 (2020) 145157

➢ Electrocatalytic performance using 3-electrode system

LSV polarization curves for full-water splitting

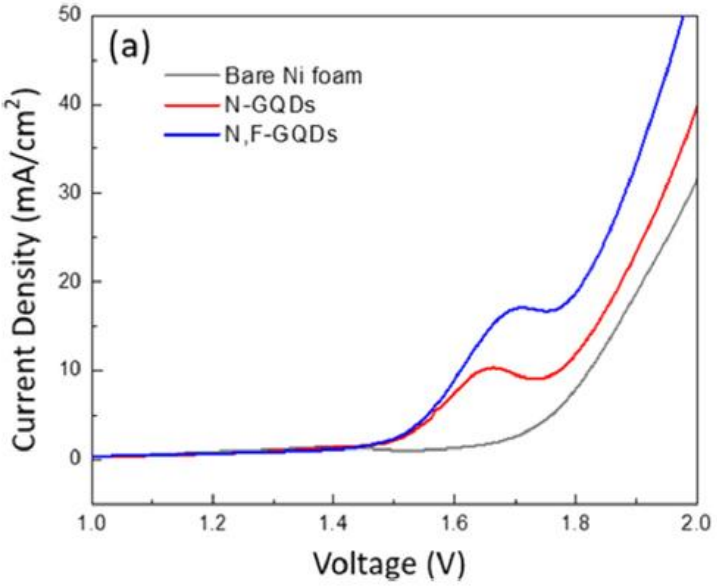

Stability test in basic condition

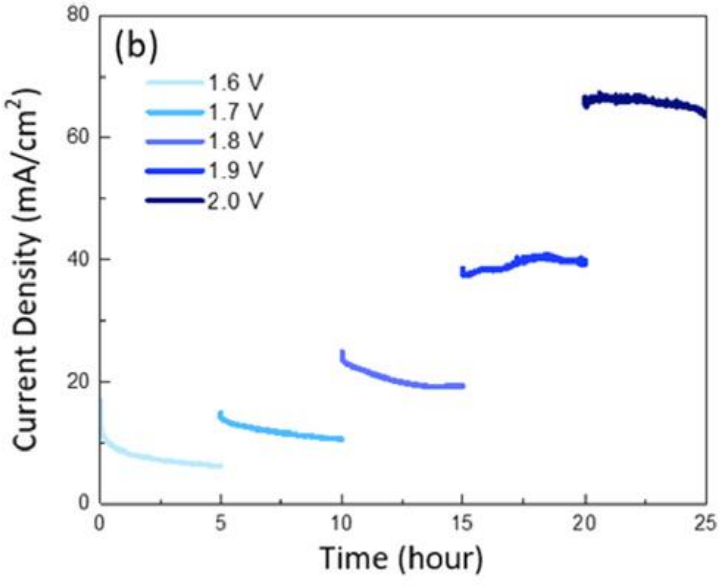

- The fabricated water splitting system comprises of bifunctional N,F-GQDs employed as an anode and cathode to facilitate both OER and HER activity and compared with asymmetric 2-electrode system consisted of N-GQDs.
- The fabricated symmetric full-cell system of N,F-GQDs needs a low cell voltage of 1.61 V to generate a water splitting current density of 10 mA cm^{-2}, whereas the N-GQDs (1.66 V), and bare Ni foam (1.8 V) based systems demanded a higher voltage to drive the same current density.
- The N,F-GQDs has accomplished the stability test for 25 h without any deficiency in the performance.
- The N,F-GQDs showed the best catalytic activity for the HER and OER due to synergistic coupling effect of N and F.

In situ Grown $CoMn_2O_4$ 3D-tetragons on Carbon Cloth: Flexible Electrodes for efficient Rechargeable Zinc-Air Battery Powered Water Splitting Systems

Published

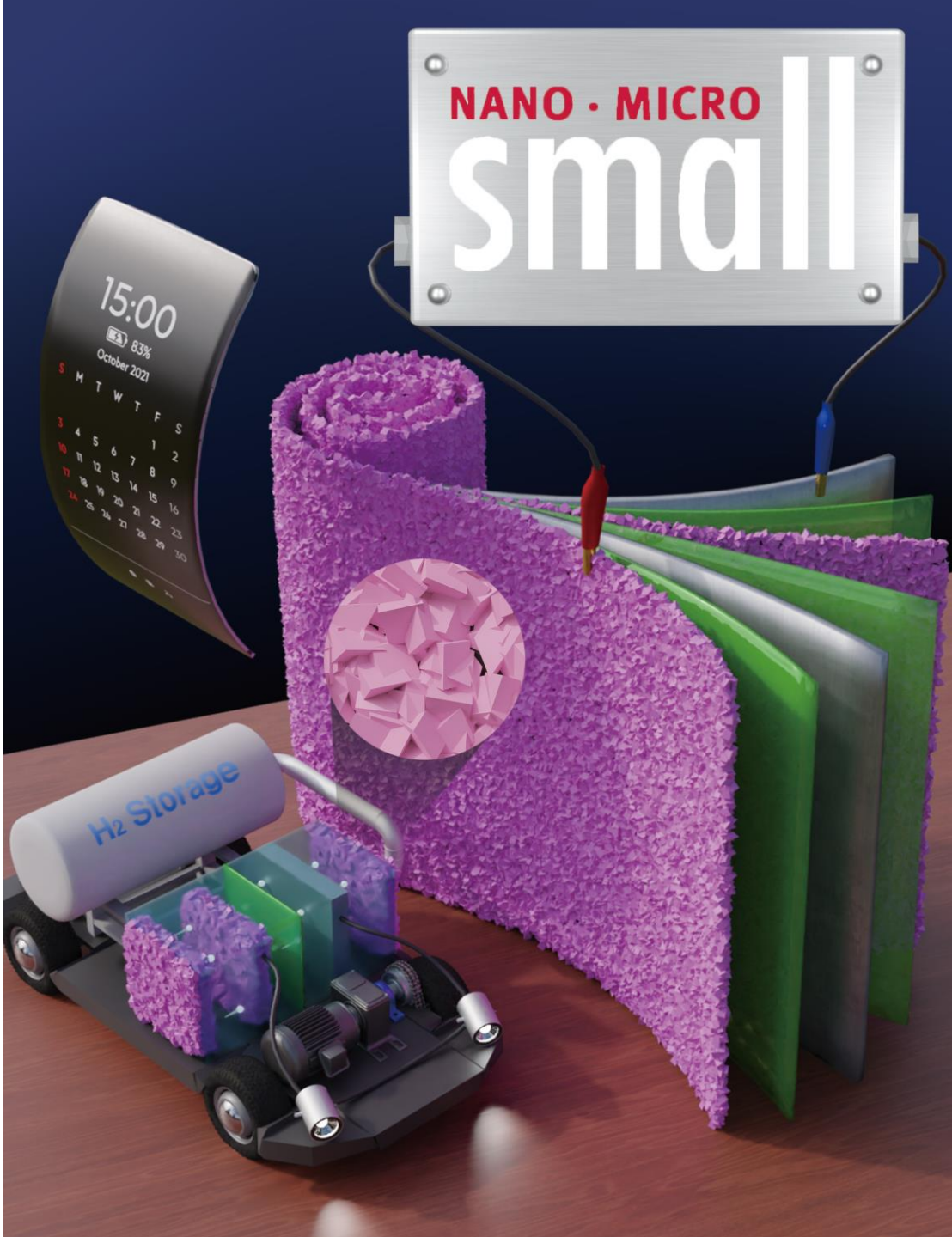
NANO · MICRO
small
15:00
83%
October 2021
H2 Storage

Zinc-air Battery Powered Water Splitting Systems

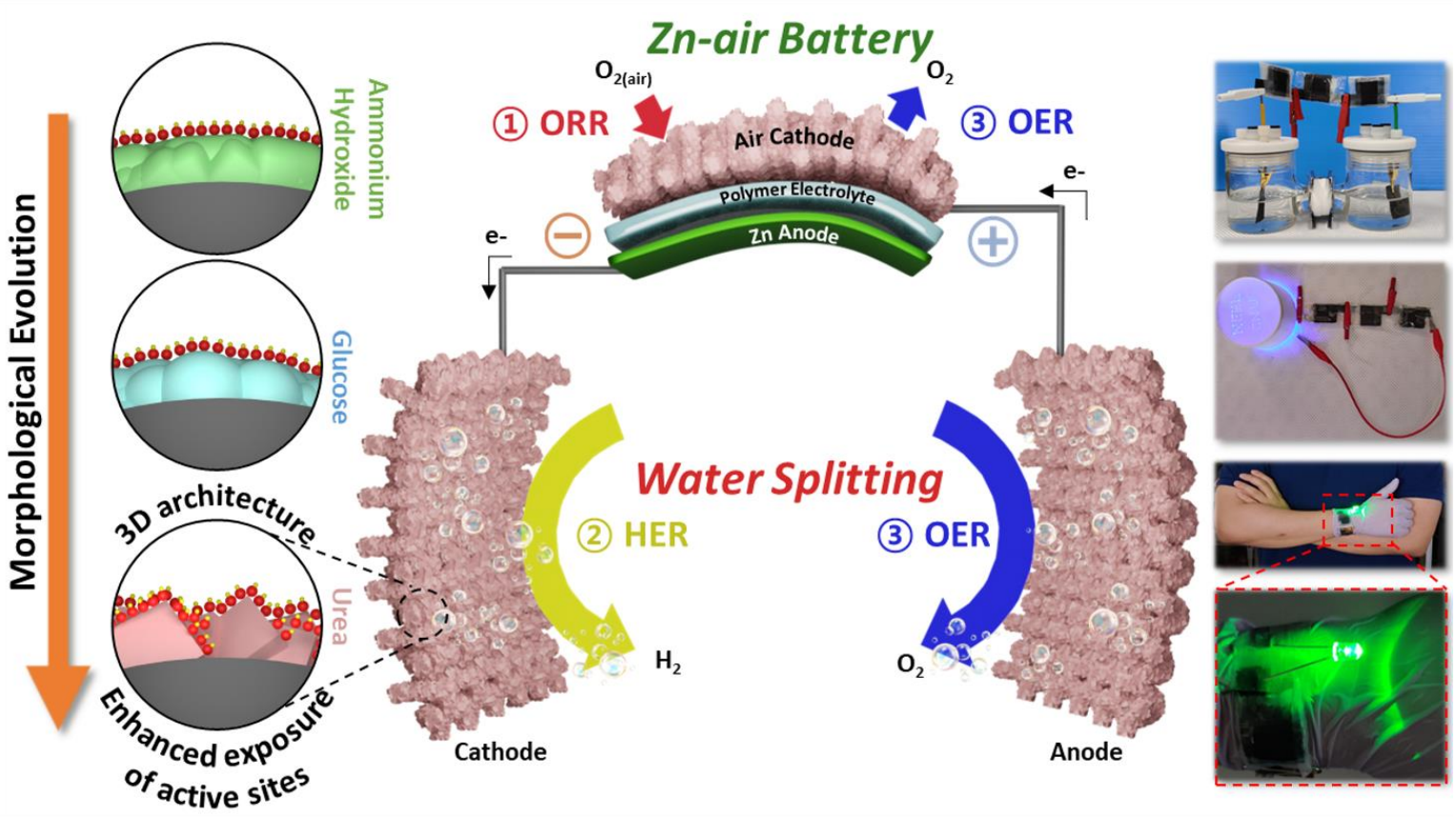

- By using in situ grown technique a flexible electrode was fabricated to be used in the electroche mical water splitting and flexible zinc-air battery.
- The prepared electrode can perform the multifunctional electrocatalytic activity as the anode a nd cathode in electrochemical water splitting and cathode in zinc-air battery.

Insitu growth mechanism of $CoMn_2O_4$ @CC

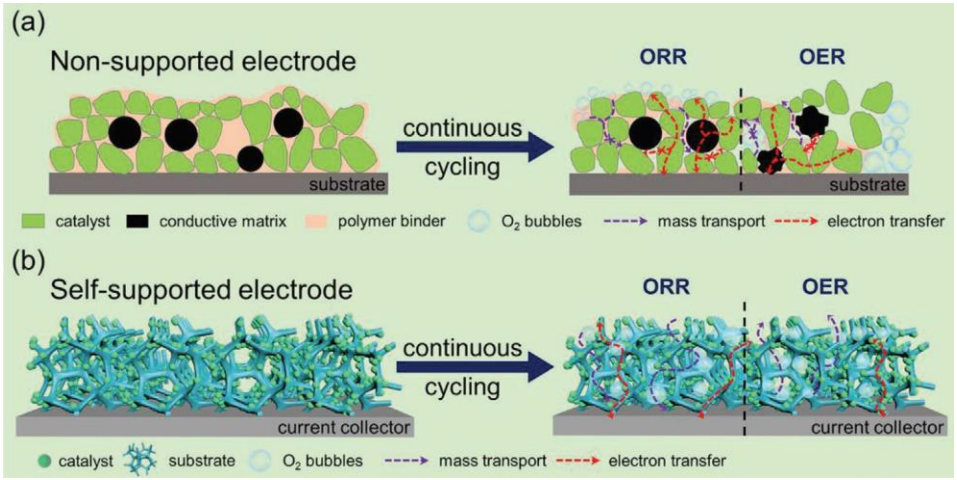

- Simplify the electrode preparation and lowers c ost.
- Provides abundant catalytic sites.
- Binding of catalytic materials and substrates is more intimate without additional binder, ensure s rapid charge transfer.

- To obtain the homogeneous particle formation over car bon cloth with good binding between the grown particl es and the carbon cloth, three different oxide sources-u rea, ammonium hydroxide and glucose were used.
- Glucose polymerized and confined the particle growth.
- Ammonium hydroxide forms metal hydroxides, which fl occulated and precipitated.
- Urea precipitated the cobalt and manganese metals in t he solution provided the OH- ions.
- Gradual increment of the solution pH with the decompo sition of urea, results in the homogenous growth of part icles.

Growth mechanism

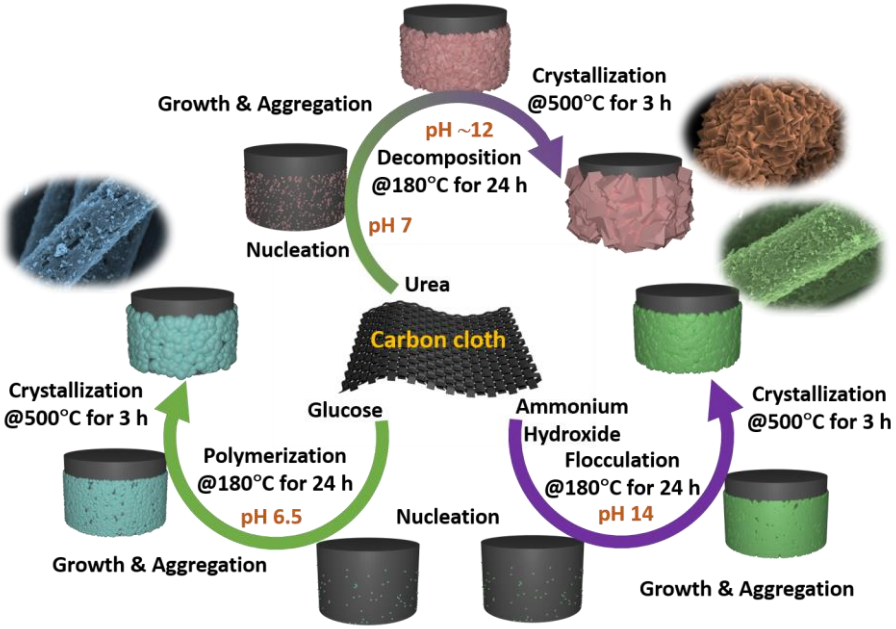

Morphology and Microstructure analysis

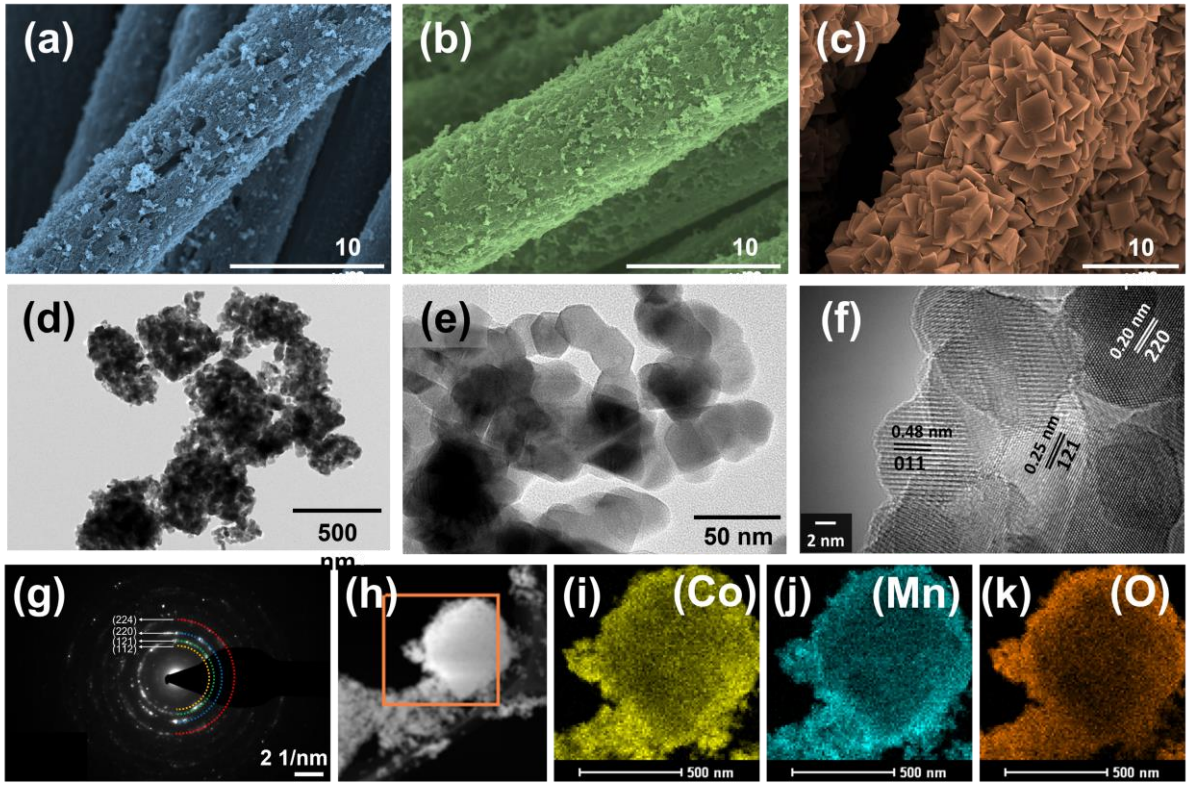

Figure 1. SEM images of (a) CMO-G@CC, (b) CMO-A@CC, (c) CMO-U@CC. (d–f) HRTEM images of CMO-U@CC at various resolutions, (g) Corresponding SAED pattern, and (h–k) Elemental mapping.

Uniform decoration of particles

- CMO-U@CC results with proper particle formation than CMO-G@CC and CMO-A@CC (Figure a-c).
- Figure f displays a well-resolved lattice fringe with interplanar spacings of 0.48 and 0.25 nm corresponding to the (011) and (121) planes of $CoMn_2O_4$.
- Elemental mapping images in Figure 1h-k validates the existence of uniformly distributed Co, Mn, and O elements in CMO-U@CC.

X-Ray-Diffraction and Photoelectron Spectroscopy

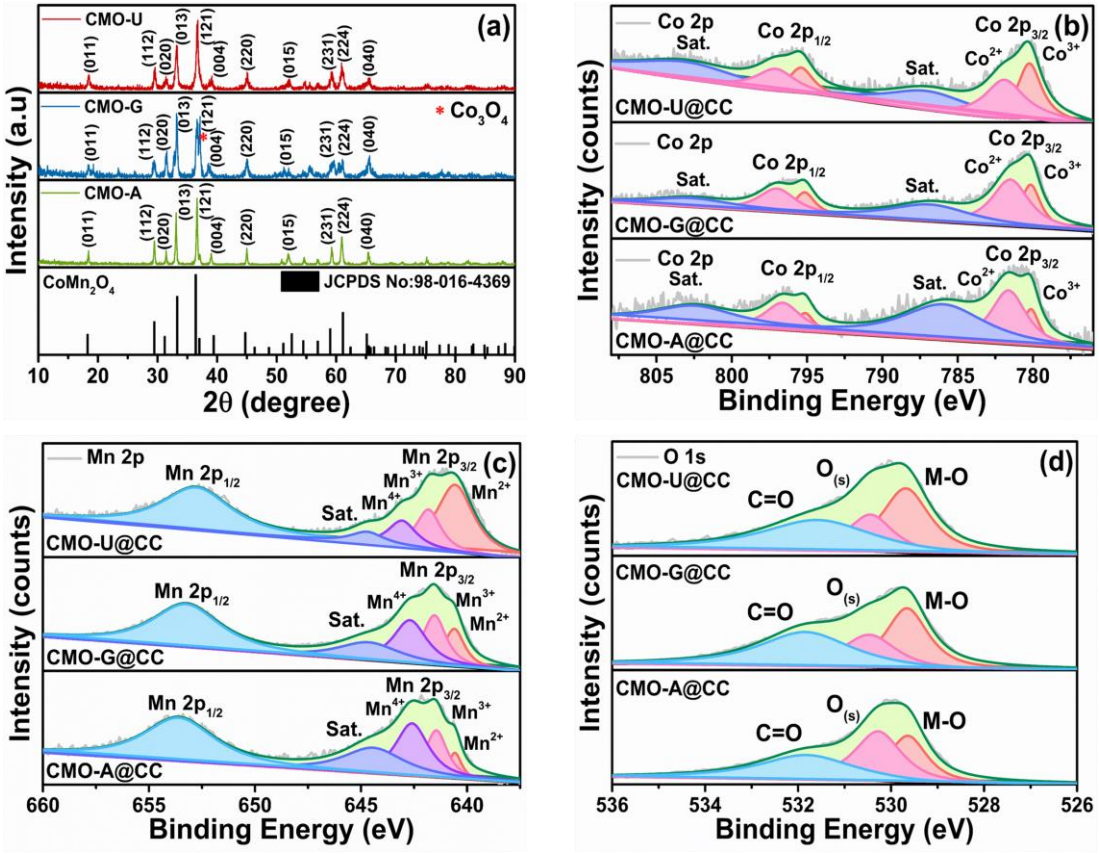

Figure 2. XRD patterns of (a) CMO-U, CMO-G and CMO-A. High-resolution XPS spectra of (b) Co 2p, (c) Mn 2p and (d) O1s in CMO -U@CC, CMO-G@CC, and CMO-A@CC.

Tetragonal $CoMn_2O_4$ structure Co^{2+} and Co^{3+}, Mn^{2+}, Mn^{3+} and Mn^{4+} and metal oxide, surface oxygen and C=O

- Observed well-defined and strong peaks of CMO-U, CMO-G, and CMO-A were indexed to the planes of tetragonal $CoMn_2O_4$ structure in the space group I 41/a md (JCPDS No: 98-016-4369).
- The oxidation states are studied with the XPS. There are Co2+ and 3+ in Co 2p spectra, Mn 2+, 3+ and 4+ in Mn 2p and metal oxide, surface oxygen and C=O are present in O 1s spectra.

Oxygen Reduction Reaction

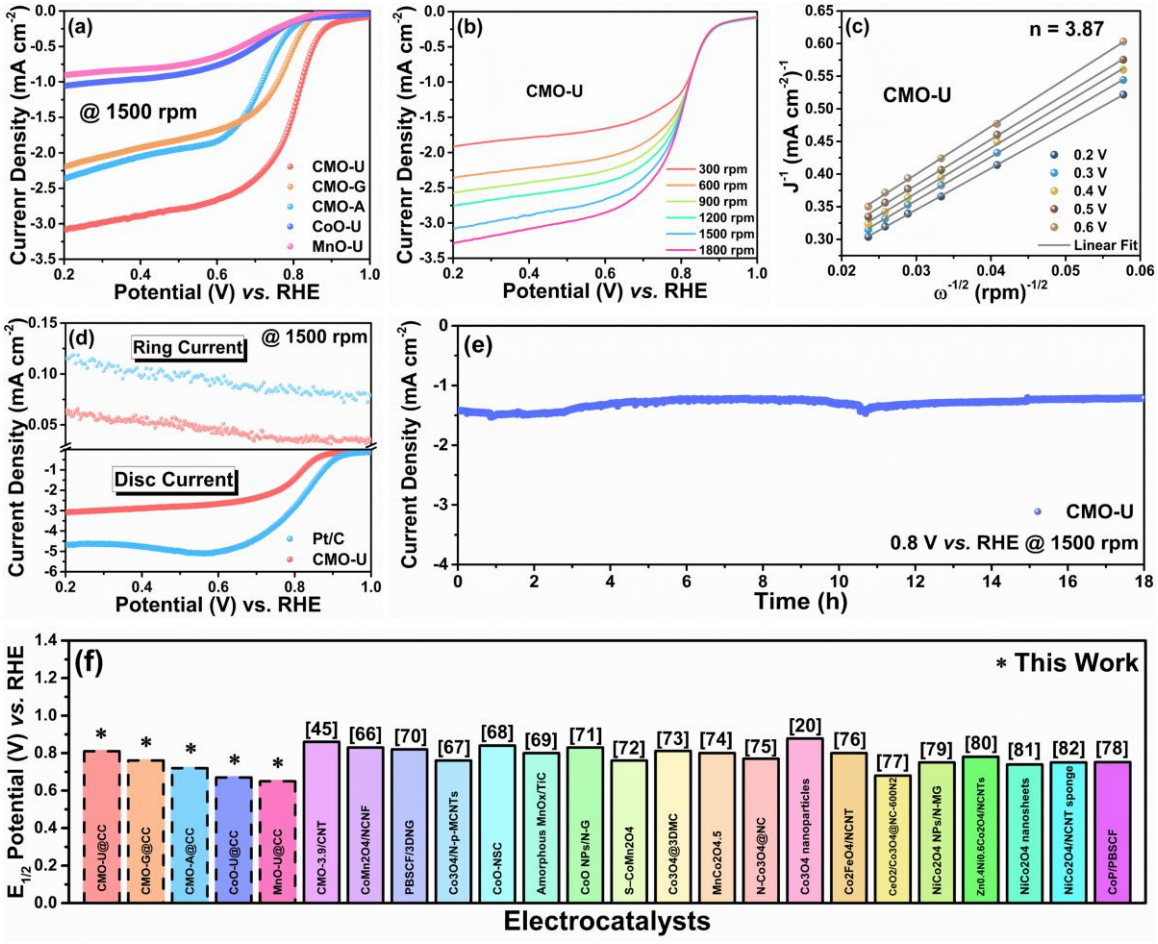

Figure 3. Polarization curves of all prepared electrodes (b) CMO-U at different rotation speeds. (c) K-L plot (d) RRDE voltammogram. (e) Chronoamperometry and (f) Comparison of ORR electrocatalytic activity with the reported oxide-based electrocatalysts.

4 e- transfer with enhanced diffusion and kinetics in CMO-U@CC

- Diffusion and kinetics of CMO-U@CC(1000 ^{o}C) was improved.
- Half-wave potential is 0.85 V
- Linearity & parallelism shows I-order kinetic reaction.
- Number of e^{-}s transferred is 4 (calculated from RRDE).
- CA evaluation carried out for 18 h exhibited the remarkable electrocatalytic stability throughout the length of analysis.
- Compared with oxide based electrocatalysts for ORR.

Oxygen Evolution Reaction

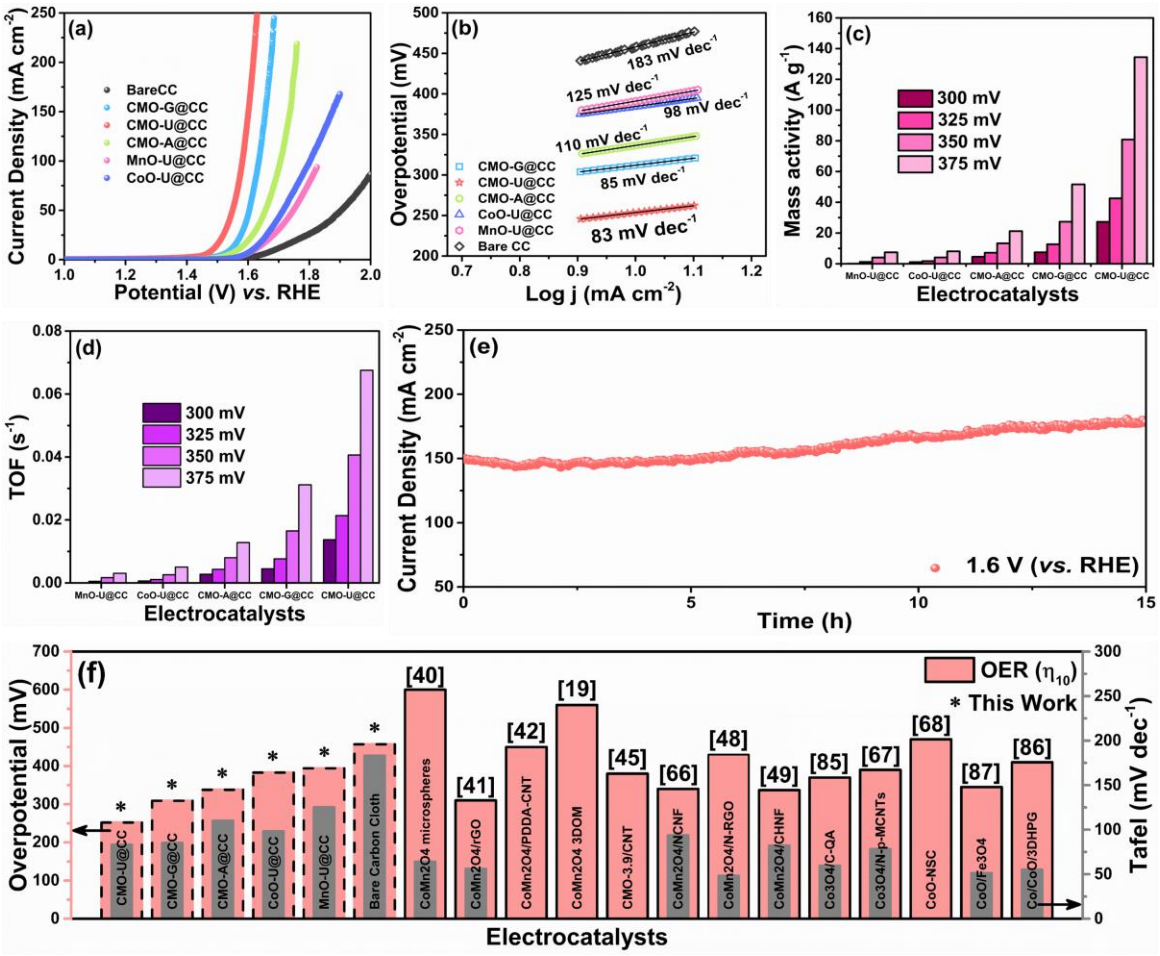

Figure 4. (a) Polarization curves (b) Tafel slopes (c) Mass activity. (d) Turn over frequency and (e) Chronoamperometry and (f) Comparison of OER electrocatalytic activity with the reported oxide-based electrocatalysts.

CMO-U@CC evolute oxygen with the improved Mass activity and Turn over frequency

- CMO-U@CC performed better relatively.
- Smaller Tafel slope indicates an increase in reaction kinetics.
- Improved Mass activity and Turn over frequency for CMO-U@CC.
- The CA analysis of the OER was carried out at a constant potential of 1.6 V for 15 h, and a steady state evolution of oxygen gas was achieved recalling the resilient strength of the electrocatalysts.
- Compared with oxide based electrocatalysts for OER.

Hydrogen Evolution Reaction

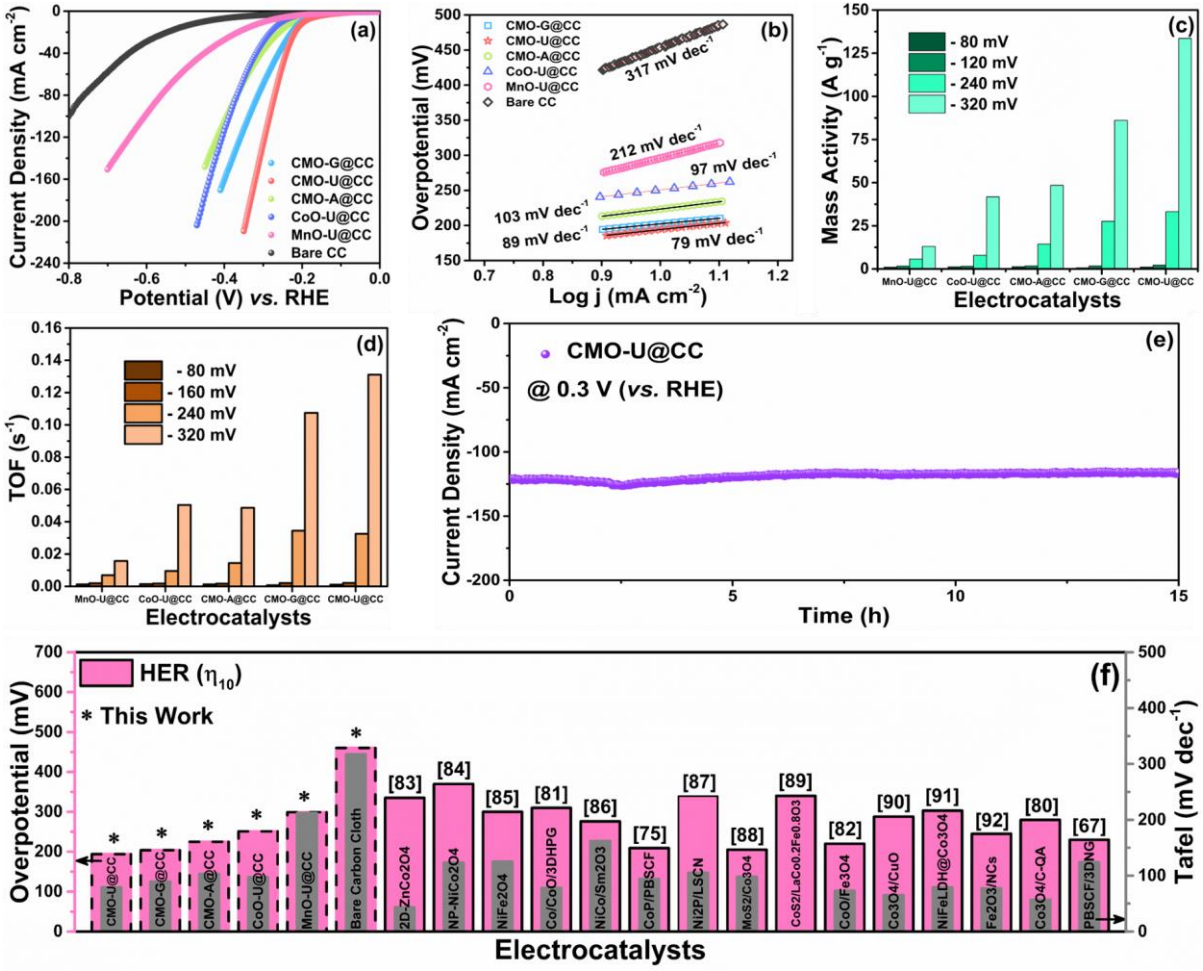

Figure 5. (a) Polarization curves (b) Tafel slopes (c) Mass activity. (d) Turn over frequency and (e) Chronoamperometry and (f) Comparison of HER electrocatalytic activity with the reported oxide-based electrocatalysts.

CMO-U@CC evolute hydrogen with the improved Mass activity and Turn over frequency

- CMO-U@CC performed better relatively.
- Smaller Tafel slope indicates an increase in reaction kinetics.
- Improved Mass activity and Turn over frequency for CMO-U@CC.
- The CA analysis of the HER was carried out at a constant potential of 0.3 V for 15 h, and a steady state evolution of hydrogen gas was achieved recalling the resilient strength of the electrocatalysts.
- Compared with oxide based electrocatalysts for HER.

Electrochemical analysis

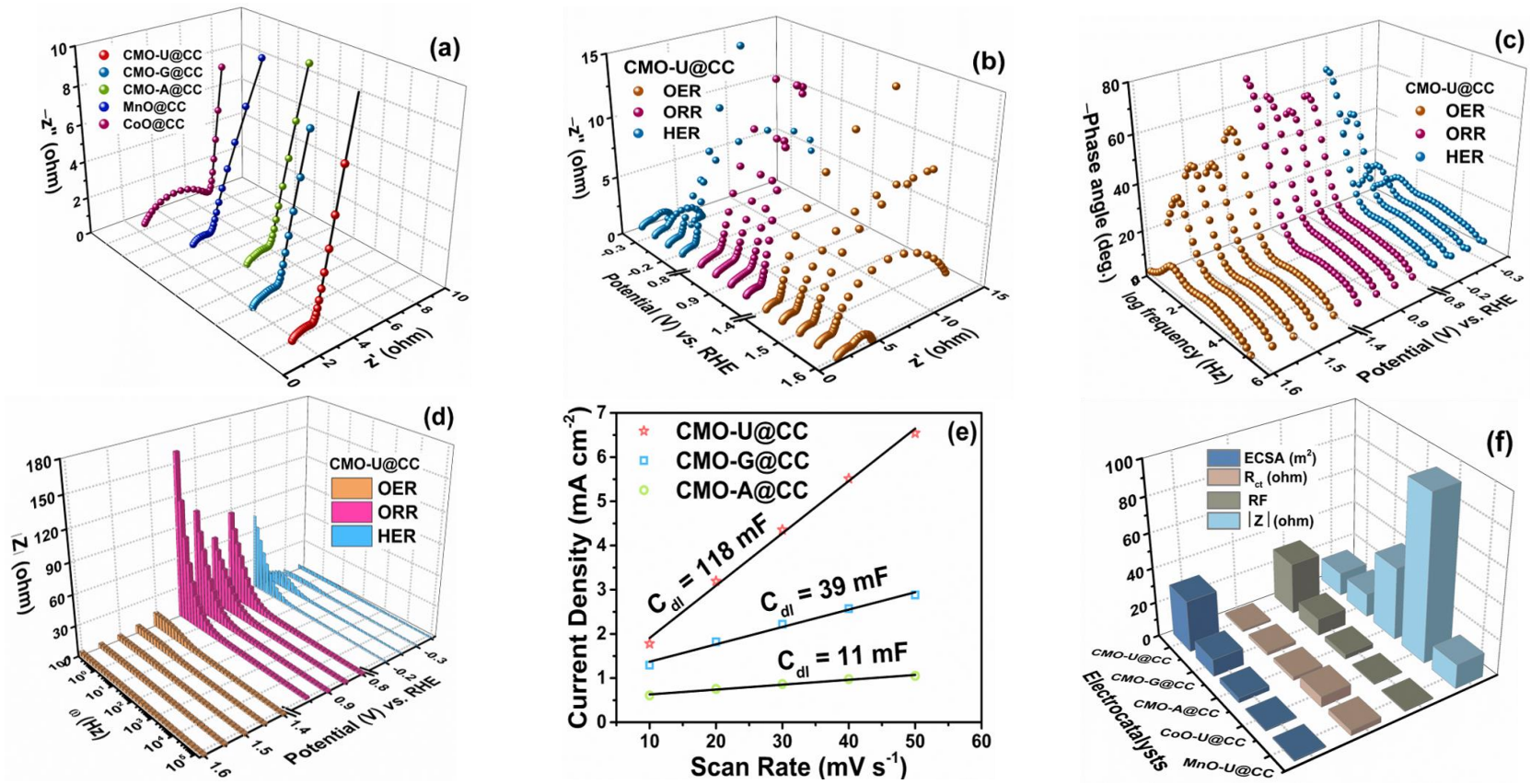

Figure 6. (a) Nyquist impedance plot (b) Potential dependent EIS (c) Phase angle vs. ω curve (d) Bode plot (|Z| vs. ω) of CMO-U@CC wrt applied potenti al (e) Peak current density vs. scan rate and (f) Comparison of ECSA, Rct, roughness factor, and impedance values of the prepared electrodes.

- In Figure a, CMO-U@CC reveals the reduced impedance. In Figure b, c and d, the decrease in impedance occurred i n the range of applied potential (vs. RHE) of the kinetic driven region during the ORR, OER, and HER with CMO-U@ CC.
- The higher Cdl value of CMO-U@CC results in the greater ECSA. The above obtained ECSA, Rct, RF, and |Z| values of all the prepared electrodes are compared in Figure 6f to get a clear picture.

Electrochemical Water splitting

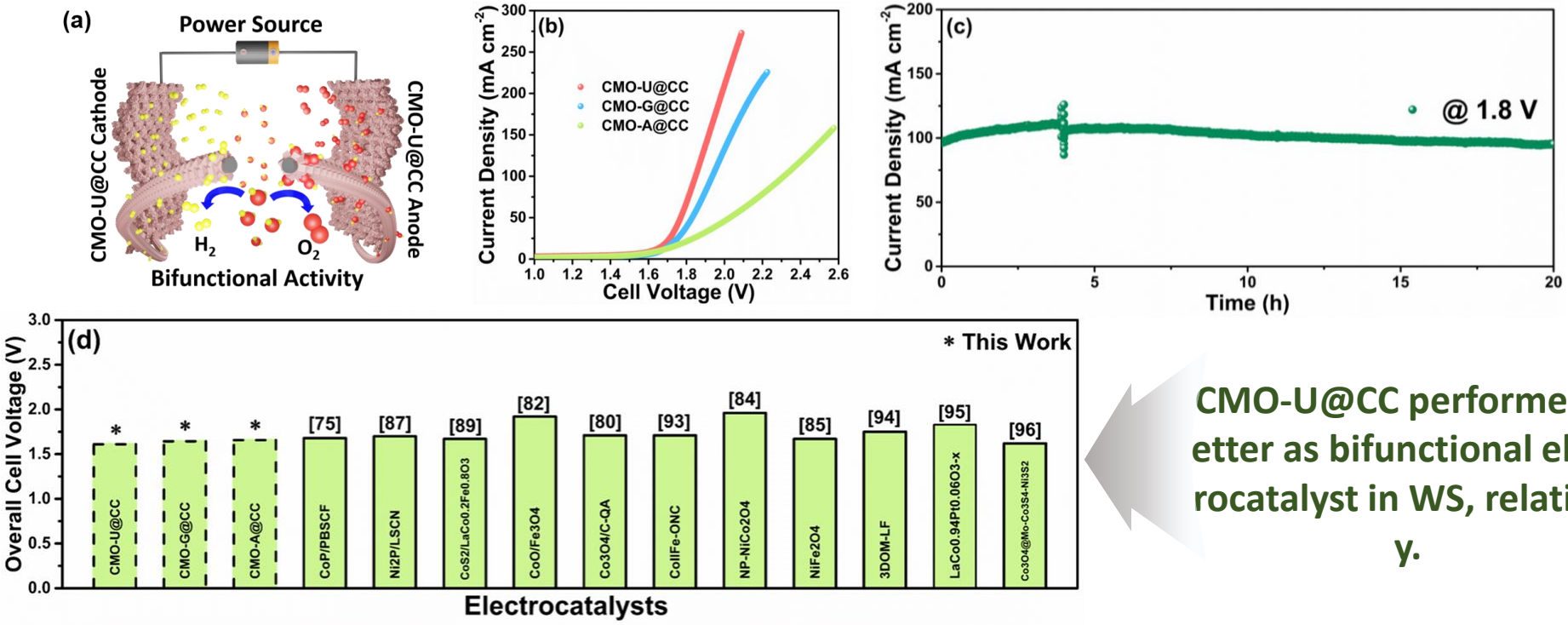

CMO-U@CC performed b etter as bifunctional elect rocatalyst in WS, relativel y.

Figure 7. (a) Schematic representation of EWS (b) LSV curves of the constructed lab scale water electrolyzer. (c) Chronoam perometry of water splitting cell (d) Comparison of water splitting activity with the reported oxide-based electrocatalysts.

- LSV curves in Figure 7b show that CMO-U@CC, CMO-G@CC, and CMO-A@CC-based EWS systems only required a n overall voltage of 1.610, 1.643, and 1.657 V, respectively, at 10 mA cm^{-2}.
- Chronoamperometric characterization was performed for 20 h to evaluate the stability of CMO-U@CC activity for EWS (Figure 7c), and the results confirmed the stability of CMO-U@CC activity for EWS.
- Compared with oxide based electrocatalysts for WS.

Zinc-air battery

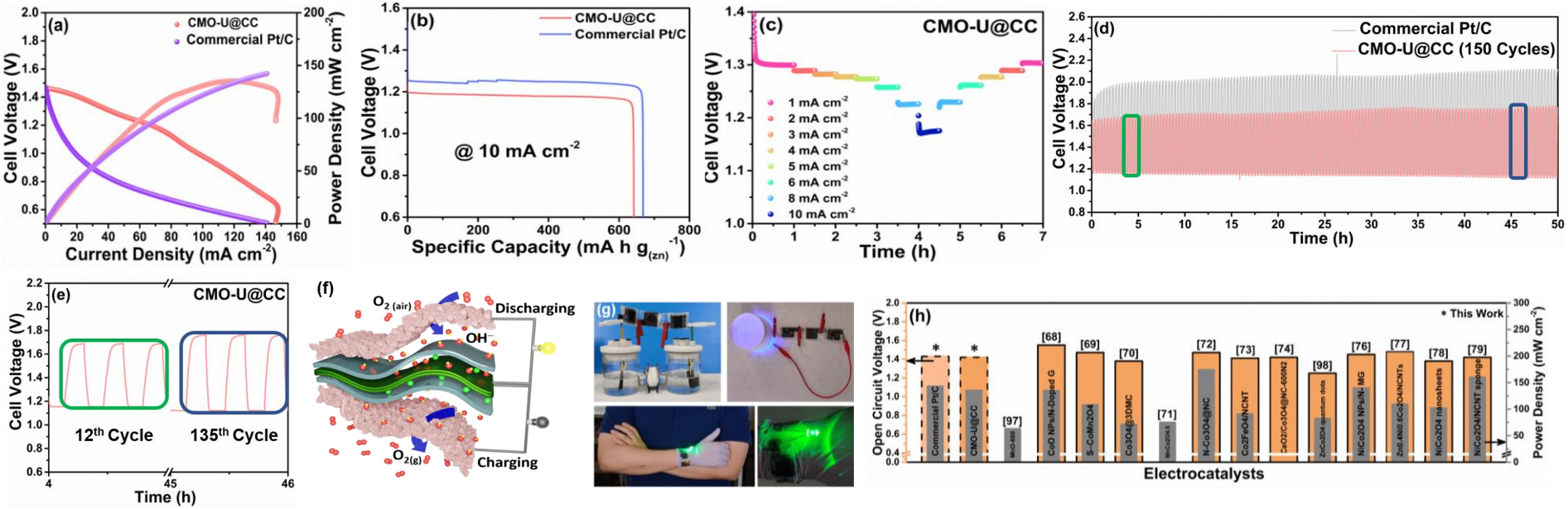

Figure 8. (a) Polarization and power density curves (b) Voltage-Specific capacity curve (c) Galvanostatic discharging profiles at different current density. (d) C harge–discharge cycles (e) Charge–discharge curves (f) Schematic representation (g) Demonstration with the flexible CMO-U@CC cathode to power the EWS and to power the LED under normal and bending condition. (h) Comparison of ZAB activity with the reported oxide- based electrocatalysts.

- CMO-U@CC air cathode delivers a maximum power density of 135 mW cm^{-2} and exhibited a specific capacity value of 641 mA h g_{zn}^{-1} compared to that of Pt/C (143 mW cm^{-2} and 667.7 mA h g_{zn}^{-1} at a current density of 10 mA cm^{-2}) (Figure 8a and 8b). Figure c proved that the CMO-U@CC air cathode is rate capable.
- The charge–discharge rest times were 10 min, and there was no much change in the voltage gap between the charge and discharge cycles of rechargeable ZAB for 50 h.
- A flexible ZAB was constructed with the Zn anode, CMO-U@CC binder free flexible cathode and PVA gel polymer electrolyte as shown in the Figure 8f. The binder free flexible ZAB in series with cathode CMO-U@CC was successfully tested as a power source for the EWS system.
- Compared with oxide based electrocatalysts for ZAB.

Carbon-Enriched Cobalt Phosphide with Assorted Nanostructure as a Multifunctional Electrode for Energy Conversion and Storage Devices

Published

Subramani Surendran,[a, c] Sathyanarayanan Shanmugapriya,[a] Yun Sung Lee,*[b] Uk Sim,*[c] and Ramakrishnan Kalai Selvan*[a]

Carbon-Enriched Cobalt Phosphide for water splitting

➢ XRD pattern and XPS spectra of Co_2P nanostructure

ChemistrySelect 2018, 3, 12303– 12313

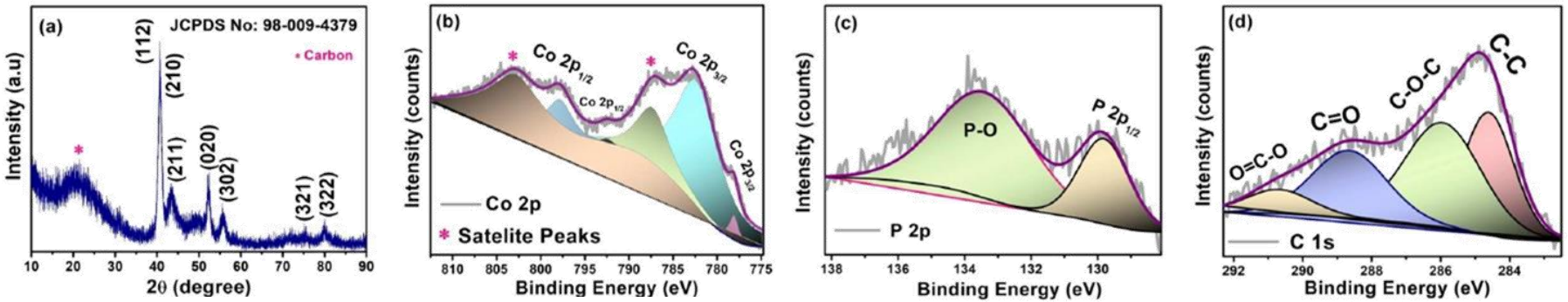

- The prepared Co_2P is phase pure with an orthorhombic structure having the space group of P- nma.
- The existence of carbon in Co_2P can be endorsed to the inclusion of cobalt acetate as the starting precursor which serves as the only recognized source of the carbon.
- The evidential presence of P-bonded cobalt atoms in cobalt phosphide may provide electron transfer channels that enrich the conductivity of the prepared Co_2P.

➢ FESEM, TEM, HRTEM and SAED pattern

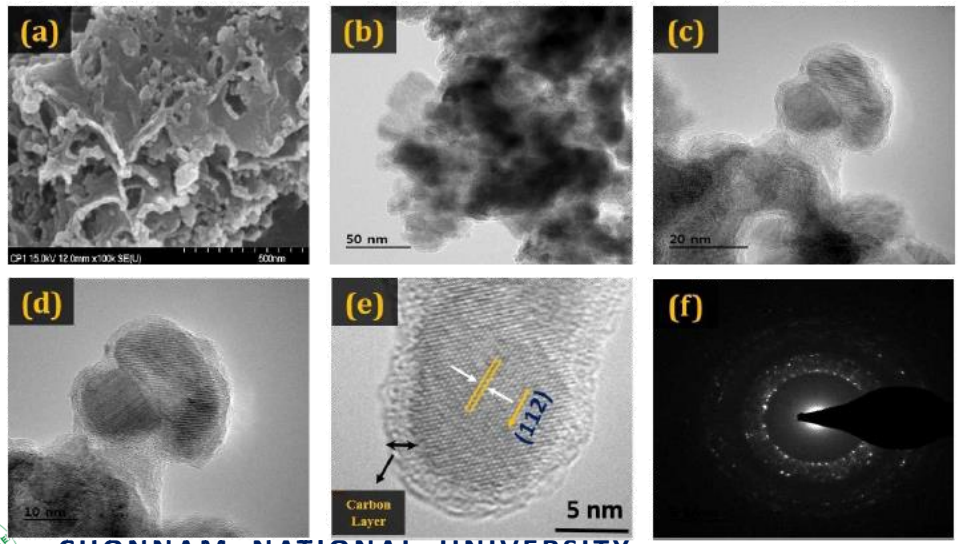

- The Co_2P/C are formed scaffold-like nanostructures, framed by uniformly embraced spherical nanoparticles.
- HRTEM images show Co_2P/C with distinct lattice fringes through interplanar distances of 0.22 nm, corresponding to the high intense (112) plane of the orthorhombic Co_2P crystal structure.
- A thin layer of carbon (~2-3 nm) coated on the surface of the individual particles.
- The SAED pattern elucidates the polycrystalline nature of the Co_2P/C nanostructures.

Carbon-Enriched Cobalt Phosphide for water splitting

ChemistrySelect 2018, 3, 12303– 12313

➢ Electrocatalytic properties for OER of Co_2P/C electrodes

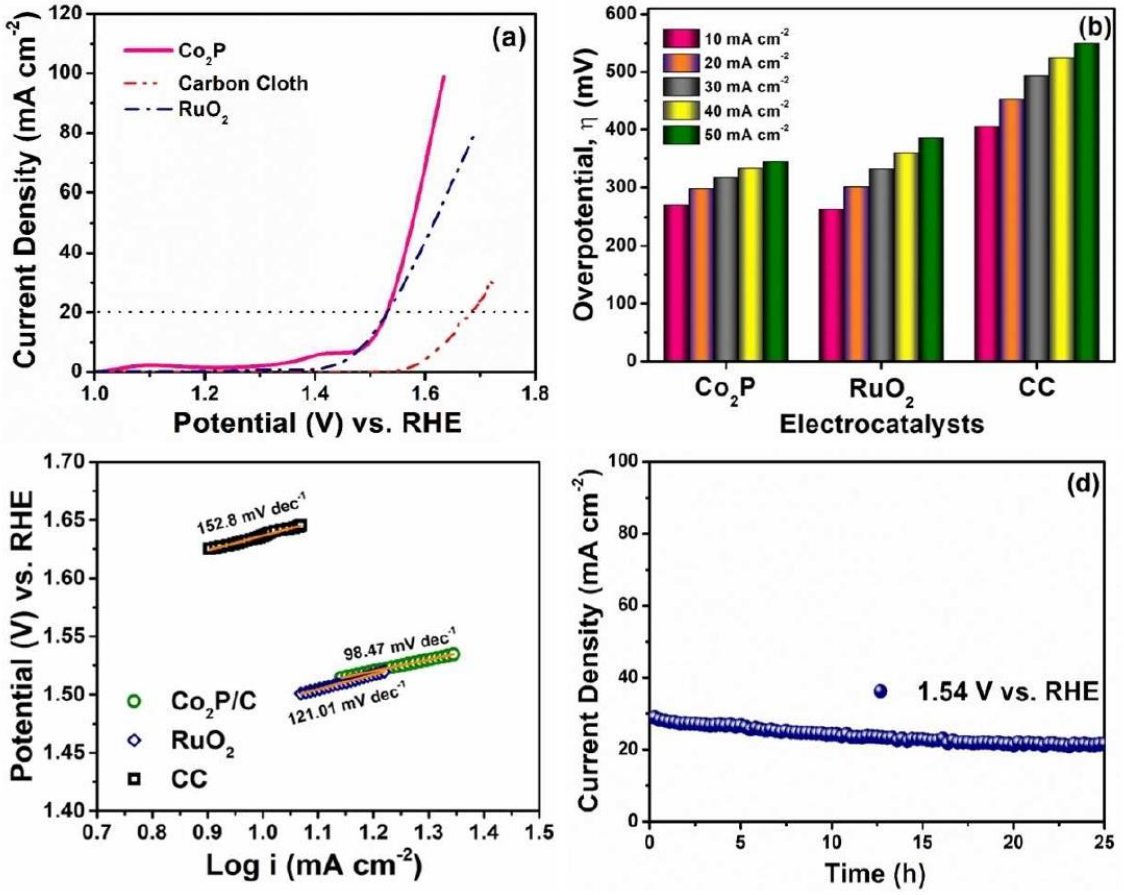

- In LSV polarization curves, two distinct peaks witnessed initially at 1.1 and 1.4 V (vs RHE) owing to the oxidation reactions associated with the Co^{2+}/Co^{3+} and Co^{3+}/Co^{4+} redox couples.
- The prepared scaffold-like Co_2P electrocatalyst has shown an excellent catalytic activity with an essential onset potential at 1.47 V (vs RHE).
- The prepared Co_2P/C electrocatalyst requisite an overpotential of 298 mV to attain an elevated current density of 20 mA cm^{-2}.
- As the potential increases, the Co_2P tends to move much straighter demanding low overpotentials of 298, 317, 333 and 345 mV at 20, 30, 40, and 50 mA cm^{-2} resulting in better catalytic activity.

- The rate determining step of Co_2P electrocatalyst was depicted to be a single-electron transfer step with a minimum Tafel slope of 98.47 mV dec^{-1}.
- The unceasing evolution of O_2 bubbles from the electrode surface and the negligible changes in the current value throughout the completion of CA scrutiny ensure the highly stable nature of the prepared Co_2P electrocatalyst for OER activity.

Carbon-Enriched Cobalt Phosphide for water splitting

ChemistrySelect 2018, 3, 12303– 12313

➢ Electrocatalytic properties for HER of Co_2P/C electrodes

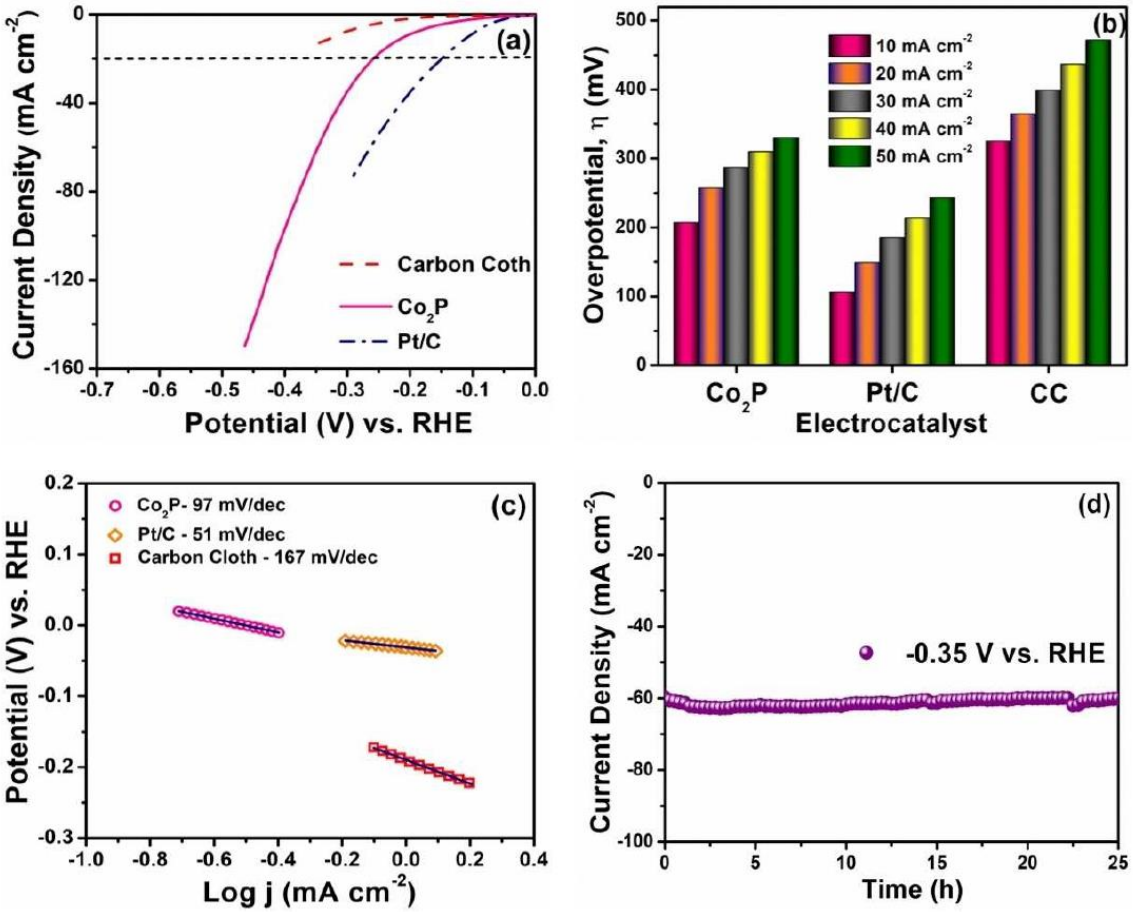

- In LSV polarization curves, the prepared scaffold-like Co_2P electrocatalyst shown an excellent catalytic activity with an essential onset potential at 0.16 V (vs RHE).
- The prepared Co_2P electrocatalyst requisite an overpotential of 257 mV to attain an elevated current density of 20 mA cm^{-2}.
- As the potential increments the Co_2P tends to move squarer demanding low overpotentials of 207, 257, 287, 310 and 330 mV at an augmented current densities of 10, 20, 30, 40, and 50 mA cm^{-2}.
- The obtained low Tafel slope of 97 mV dec^{-1} for Co2P electrocatalyst transpires the rate-determining step as the discharge reaction.

- The CA analysis was studied for a constant potential of -0.35 V (vs RHE) for 25 hours, which illustrated a slight rise in the current rather than a drop elucidating the extraordinary strength of the Co_2P electrocatalyst.

Carbon-Enriched Cobalt Phosphide for water splitting

ChemistrySelect 2018, 3, 12303– 12313

- The schematic illustration of the assembled lab-scale water electrolyzer

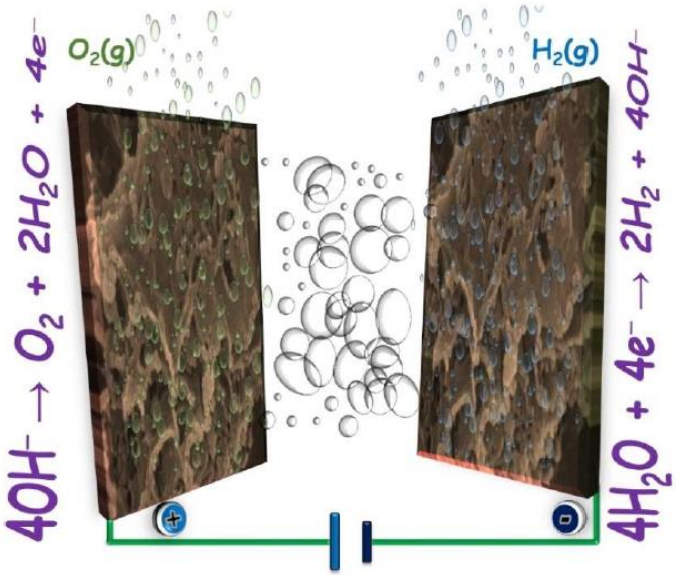

- The lab-scale water electrolyzer was assembled by a two-electrode set up encompassing bifunctional Co_2P/C electrode as both anode and cathode.

- LSV polarization curves and CA curves of the device

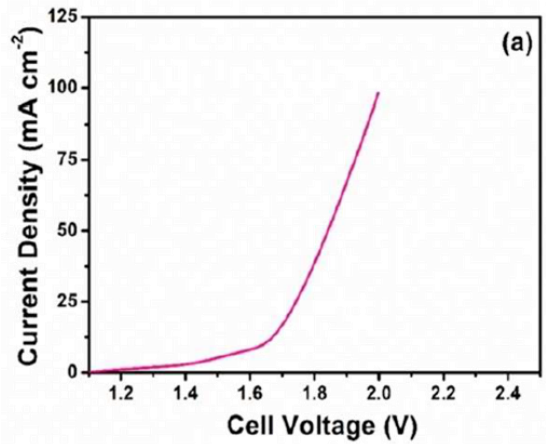

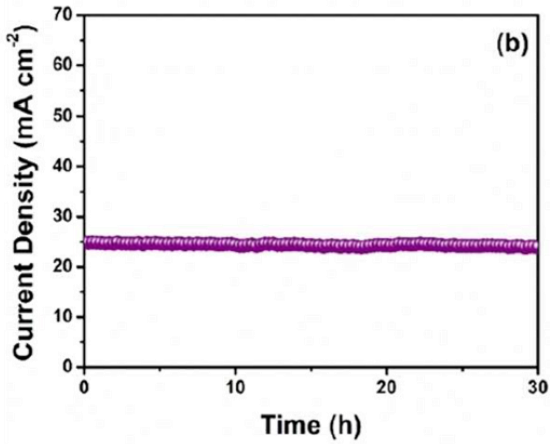

- The assembled water electrolyzer insists that a minimum potential of 1.63 V is necessary to attain a water-splitting current density of 10 mA cm^{-2}, resulting in the evolution of large troops of oxygen and hydrogen gas bubbles from both the surfaces of the electrodes.
- The CA analysis of the water electrolyzer was completed at a static potential (1.75 V), and a steady state of evolution of gas was achieved for about 30 hours recalling the resilient strength of the Co_2P electrode.